Atmos. Meas. Tech., 4, 1929–1935, 2011
www.atmos-meas-tech.net/4/1929/2011/
doi:10.5194/amt-4-1929-2011

Atmospheric Measurement Techniques

Observation of slant column NO_2 using the super-zoom mode of AURA-OMI

L. C. Valin[1], A. R. Russell[1], E. J. Bucsela[2], J. P. Veefkind[3,4], and R. C. Cohen[1,5]

[1]College of Chemistry, University of California Berkeley, Berkeley, CA 94720, USA
[2]SRI International, Menlo Park, CA 94025, USA
[3]Royal Netherlands Meteorological Institute (KNMI), De Bilt, The Netherlands
[4]Delft University of Technology, Delft, The Netherlands
[5]Department of Earth and Planetary Sciences, University of California Berkeley, Berkeley, CA 94720, USA

Received: 8 February 2011 – Published in Atmos. Meas. Tech. Discuss.: 29 March 2011
Revised: 12 August 2011 – Accepted: 30 August 2011 – Published: 19 September 2011

Abstract. We retrieve slant column NO_2 from the super-zoom mode of the Ozone Monitoring Instrument (OMI) to explore its utility for understanding NO_x emissions and variability. Slant column NO_2 is operationally retrieved from OMI (Boersma et al., 2007; Bucsela et al., 2006) with a nadir footprint of $13 \times 24\,km^2$, the result of averaging eight detector elements on board the instrument. For 85 orbits in late 2004, OMI reported observations from individual "super-zoom" detector elements (spaced at $13 \times 3\,km^2$ at nadir). We assess the spatial response of these individual detector elements in-flight and determine an upper-bound on spatial resolution of 9 km, in good agreement with on-ground calibration (7 km FWHM). We determine the precision of the super-zoom mode to be 2.1×10^{15} molecules cm^{-2}, approximately a factor of $\sqrt{8}$ lower than an identical retrieval at operational scale as expected if random noise dominates the uncertainty. We retrieve slant column NO_2 over the Satpura power plant in India; Seoul, South Korea; Dubai, United Arab Emirates; and a set of large point sources on the Rihand Reservoir in India using differential optical absorption spectroscopy (DOAS). Over these sources, the super-zoom mode of OMI observes variation in slant column NO_2 of up to 30 × the instrumental precision within one operational footprint.

1 Introduction

Nitrogen oxides ($NO_x \equiv NO + NO_2$) exhibit strong control over tropospheric ozone production and HO_x ($HO_2 + RO_2 + HO$) cycling. Despite a relatively short chemical lifetime ($\tau_{NO_x} \sim 1.5\,h - 1$ day in the planetary boundary layer), NO_x emitted locally can result in perturbations to atmospheric composition that extend for hundreds of kilometers, in part due to atmospheric processing that stores and releases NO_x, but also in part due to the magnitude of the source being many e-folds in excess of the global background.

Satellite-based UV/Visible mapping spectrometers provide a comprehensive view of the global and regional patterns of NO_2 columns (e.g. Jaegle et al., 2005; Richter et al., 2005; Russell et al., 2010). Interpretation of these observations has primarily been via chemical transport models (grid spacing ≈ 100 km) that assume chemical processing is accurately represented (e.g. Martin et al., 2003; Toenges-Schuller et al., 2006; Konovalov et al., 2006; Kim et al., 2006). Many of these models have resolution that is coarse compared to both the e-folding decay length of an NO_2 plume and the spatial resolution provided by the satellite instruments. High resolution observations offer the possibility of direct measurement of the spatial gradients in the NO_2 column in regions where such gradients depend on the chemical loss rates of NO_2 more strongly than on emissions (e.g. Heue et al., 2008). The resolution needed for such analyses is still a subject of research (e.g. Loughner et al., 2007; Valin et al., 2011); however, it seems likely to be in the range of 3–10 km.

Here we use observations from OMI (Levelt et al., 2006a,b) to retrieve slant column NO_2 at high spatial resolution. We test the spatial resolution of the OMI super-zoom mode (Sect. 3), assess the uncertainty of super-zoom observations (Sect. 4), and then retrieve slant column NO_2 over several source types (Sect. 5). We discuss the implications of the enhanced spatial resolution on our understanding of NO_x emission sources and the variability of atmospheric NO_2 using observations of Dubai, UAE (Sect. 6).

Correspondence to: R. C. Cohen
(rccohen@berkeley.edu)

Published by Copernicus Publications on behalf of the European Geosciences Union.

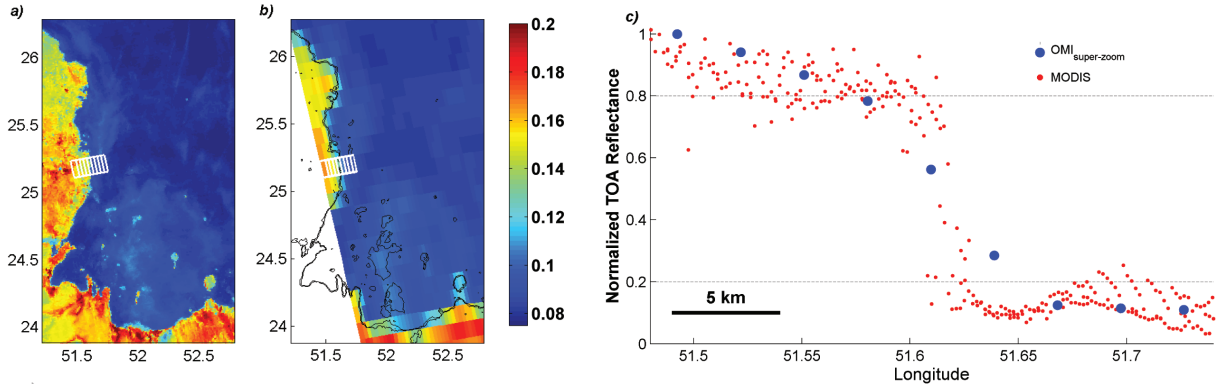

Fig. 1. Top-of-atmosphere reflectance (459–479 nm) observed by **(a)** MODIS and **(b)** the super-zoom mode of OMI over Qatar on 19 November 2004. **(c)** Normalized top-of-atmosphere reflectance observed by MODIS (red) and OMI (blue) along a transect perpendicular to the Qatari coastline – white boxes, **(a–b)**.

2 Methods

OMI sits aboard the sun-synchronous, polar-orbiting NASA Aura satellite (Schoeberl et al., 2006), measuring solar and backscattered UV/Visible radiance with a standard operational footprint of $13 \times 24\,km^2$ at nadir, an average of eight detector elements (Levelt et al., 2006a,b). OMI also has the ability to operate in a super-zoom mode where the detector elements are not averaged on board. From 1 October 2004 to 31 December 2004, OMI performed 85 super-zoom orbits, 42 of which reported observations at nadir. Due to data transmission constraints, this increase in spatial sampling requires a corresponding decrease in spatial coverage such that a single super-zoom nadir orbit covers only 180 km of the 2600 km operational-mode swath width.

We use the level 1b calibrated, wavelength-corrected OMI radiance (OML1BRVZ, OML1BRVG v.3) and solar irradiance (OML1BRR v.3) data recorded on the Goddard Earth Sciences Data and Information Services Center (GES-DISC, http://disc.sci.gsfc.nasa.gov/Aura/data-holdings/OMI) (Van den Oord et al., 2006; Dobber et al., 2008). Observed earthshine spectra are divided by the average of solar spectra from 2005 to obtain top-of-atmosphere reflectance spectra. It has been shown that the averaging of solar spectra reduces noise and detector anomalies known as "striping" in the NO_2 retrieval (Celarier et al., 2008; Dobber et al., 2008). We apply a de-striping algorithm to retrieved slant column NO_2 following Boersma et al. (2007).

We have attempted to emulate the operational retrievals (Boersma et al., 2007; Bucsela et al., 2006). We retrieve slant column NO_2 by performing a DOAS linear least squares fit (Platt and Stutz, 2008; Wenig et al., 2005) of an NO_2 cross section (Vandaele et al., 2002), an O_3 cross section (Bogumil et al., 2001), a Ring spectrum (Chance and Spurr, 1997; Chance and Kurucz, 2010), a water vapor cross section (Harder and Brault, 1997), and a third-order polynomial to the logarithm of the observed reflectance. We perform the fit over the 405–465 nm spectral window.

3 Spatial resolution of OMI super-zoom mode

On-ground calibration measurements determined the footprint of a point light source to be near-Gaussian, spanning 2.3 detector row elements at nadir (7 km FWHM) (Dobber et al., 2006). To determine an in-flight value, we compare the decay of MODIS and OMI broadband (459–479 nm) top-of-atmosphere reflectance over the Qatari coastline on 19 November 2004 (Fig. 1a). MODIS reflectance is reported at a resolution of $500 \times 500\,m^2$. By comparing the MODIS and OMI observed reflectance across a sharp transition, such as a coastline, we can deduce a value for the spatial resolution of OMI. For a single transect (Fig. 1c), MODIS observations decrease in normalized reflectance from 0.8 to 0.2 over 3 km, a decrease that OMI observes over 9 km. Additionally, the width of an observed enhancement in NO_2 directly over and downwind of an isolated NO_x source is no wider than 6–9 km FWHM (*PP4*, Fig. 2b). Both of these in-flight tests provide an upper bound on instrumental spatial resolution (∼9 km) that is in good agreement with on-ground calibration (7 km FWHM (Dobber et al., 2006).

4 Uncertainty in slant column NO_2

Figure 2 shows slant column NO_2 retrieved over the Arabian Peninsula and the Indian Ocean from a super-zoom mode orbit on 21 November 2004. To assess the uncertainty in retrieved slant column NO_2, we use a method similar to Boersma et al. (2007). We find that slant column NO_2 retrieved at operational resolution is normally distributed with $1\,\sigma$ variability of 0.8×10^{15} molecules cm^{-2} over the remote ocean and 0.6×10^{15} molecules cm^{-2} over the remote desert (Fig. 2c), well within the range of values determined previously (Boersma et al., 2007). The precision of slant column NO_2 retrieved from the super-zoom mode is approximately a factor of $\sqrt{8}$ worse, which is expected for a system

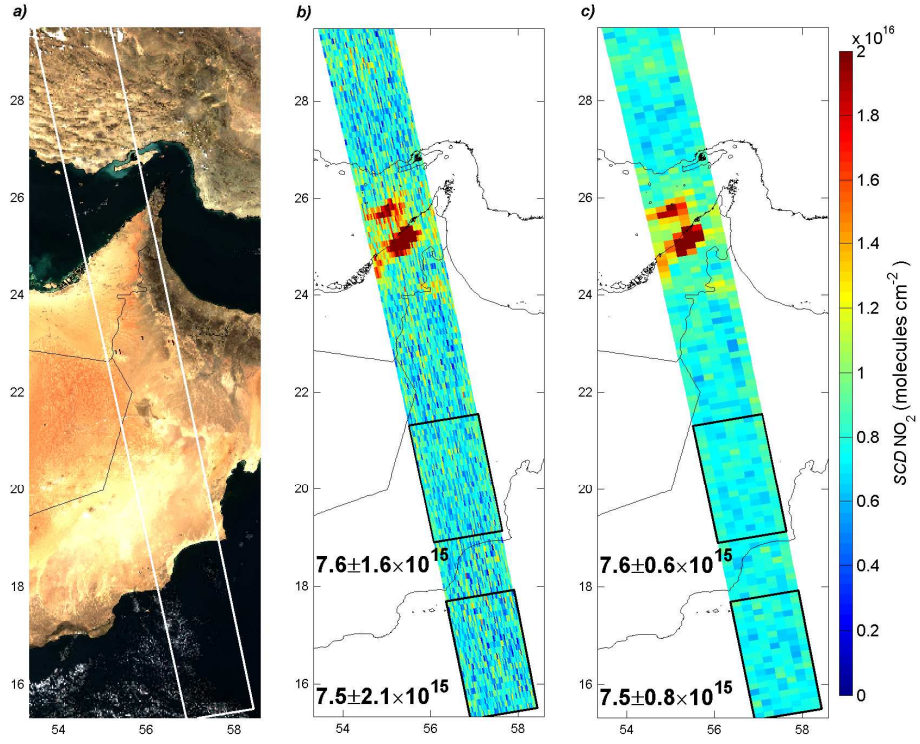

Fig. 2. **(a)** MODIS RGB image, **(b)** super-zoom slant column NO_2, and **(c)** operational-scale slant column NO_2 over the eastern Arabian Peninsula on 21 November 2004. The mean and $1\,\sigma$-uncertainty of slant column NO_2 retrieved from super-zoom and operational-scale observations over the remote ocean and desert are reported.

with 8 fewer measurements and dominated by random noise (Fig. 2b).

The NO_2 fit error computed from DOAS residuals does not increase by a factor of $\sqrt{8}$ for super-zoom observations (not shown) indicating that there are systematic residuals not reduced by averaging. While the origin of these systematic residuals is unknown, we speculate that there is slight spectral misalignment in the DOAS fitting procedure. One possible explanation for this misalignment is the lack of a shift and squeeze adjustment to improve the spectral calibration of individual spectra. However, the magnitude of any uncertainty that remains is negligible in comparison to the signal observed over sources of interest (Fig. 3)

5 Slant column NO_2 from OMI super-zoom mode

To illustrate performance of OMI in super-zoom mode and to indicate the potential for new science to emerge with high spatial resolution observations, we retrieve slant column NO_2 over the Rihand Reservoir in India, Seoul, South Korea and Sarni, Madhya Pradesh, India (Table 1). These regions highlight the super-zoom observations over a set of large point sources (Rihand), a megacity (Seoul), and a small point source (Sarni). We compare the super-zoom observations to the average of six operational-scale overpasses retrieved in the same manner. These operational resolution observations were made between the months of October and December from 2005–2007 on days when the selected region was cloud-free and nadir to the spacecraft (Table 1). We use MODIS reflectance observations, taken aboard the Aqua platform, to serve as independent visual confirmation that the selected scenes are cloud-free.

Over the Rihand Reservoir (Fig. 3a–d), the super-zoom mode distinguishes three maxima in slant column NO_2 directly over or slightly downwind of three large coal-fired power plants. This variability is not detectable with the $13 \times 24\,km^2$ operational footprint, which only observes one local maximum. Within a single operational-scale footprint, the super-zoom mode observes variation of up to 6.1×10^{16} molecules cm^{-2}, nearly 30 times larger than the instrumental precision over remote ocean. In the average of six operational-scale observations, the spatial detail is increased, but the spatial contrast observed (Fig. 3d, $1\,\sigma = 0.6 \times 10^{16}$ molecules cm^{-2}) is a factor of 2.3 less than that observed by the super-zoom mode (Fig. 3b, $1\,\sigma = 1.4 \times 10^{16}$ molecules cm^{-2}). Furthermore, the six-orbit average is only able to distinguish one maximum that is 2 times smaller than that observed on a single day.

Over Seoul, Korea (Fig. 3e–h), a maximum in slant column NO_2 (Fig. 3f) is observed approximately 12 km to the east of downtown Seoul with the signal decreasing from

Table 1. Dates and regions for which slant column NO_2 was retrieved.

	Rihand, India	Seoul, Korea	Sarni, India	Dubai, UAE
Latitude and Longitude	82.5–83.5° E 23.6–24.5° N	126.7–127.7° E 37.05–37.95° N	77.7–78.7° E 21.5–22.5° N	55.0–55.7° E 24.9–25.5° N
Date of super-zoom observations	23 Nov 2004	21 Nov 2004	19 Nov 2004	21 Nov 2004
Dates in six-orbit average	1 Nov 2005 10 Nov 2005 17 Nov 2005 19 Nov 2005 26 Nov 2005 5 Dec 2005	23 Oct 2005 8 Nov 2005 12 Oct 2006 11 Nov 2006 20 Nov 2006 7 Nov 2007	30 Oct 2005 6 Nov 2005 22 Nov 2005 8 Dec 2005 18 Nov 2006 11 Dec 2006	23 Oct 2005 30 Oct 2005 1 Nov 2005 8 Nov 2005 1 Dec 2005 3 Dec 2005

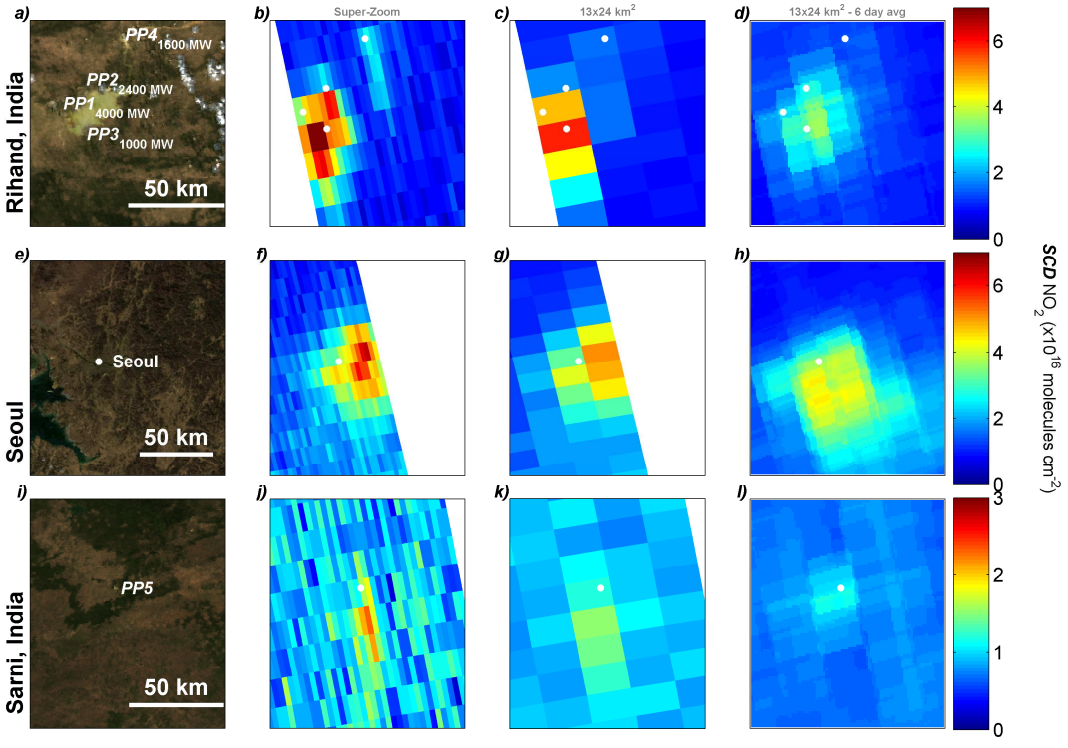

Fig. 3. MODIS RGB image, slant column NO_2 retrieved from OMI super-zoom and operational resolution observations, and from six operational resolution observations over the Rihand Reservoir in India **(a–d)**, Seoul, South Korea **(e–h)**, and Sarni, India **(i–l)**. Power plants located around the Rihand Reservoir include Singrauli and Vindhyachal (PP1 – 4200 MW), Anpara and Hindalco (PP2 – 2400 MW), Rihand (PP3 – 1000 MW pre-2006), and Obra (PP4 – 1600 MW). Power plants around Sarni, India **(i)**, include Satpura generating station (PP5).

the maximum to near-background over a distance of 30-50 km. While the operational-scale retrieval captures the general structure of the Seoul urban plume (Fig. 3g), the super-zoom mode captures variation of slant column NO_2 of up to 3×10^{16} molecules cm^{-2} (50 %) within a single operational-scale pixel. The six-orbit operational-resolution average (Fig. 3h) is much smoother than that observed in a single day, an effect of variable daily meteorology that smoothes the average.

Super-zoom observations capture a maximum in slant column NO_2 directly to the south of the Satpura Power Plant in Sarni, India (Fig. 3j; 2.2×10^{16} molecules cm^{-2}), a value that is seven times larger than the variability and average observed over the remote ocean on the same overpass. At operational-scale, both single- and six-orbit average (Fig. 3k–l), the enhancement is modest relative to the surrounding background (∼20 %).

These observations demonstrate that the instrumental noise of OMI is not the limiting factor in producing high

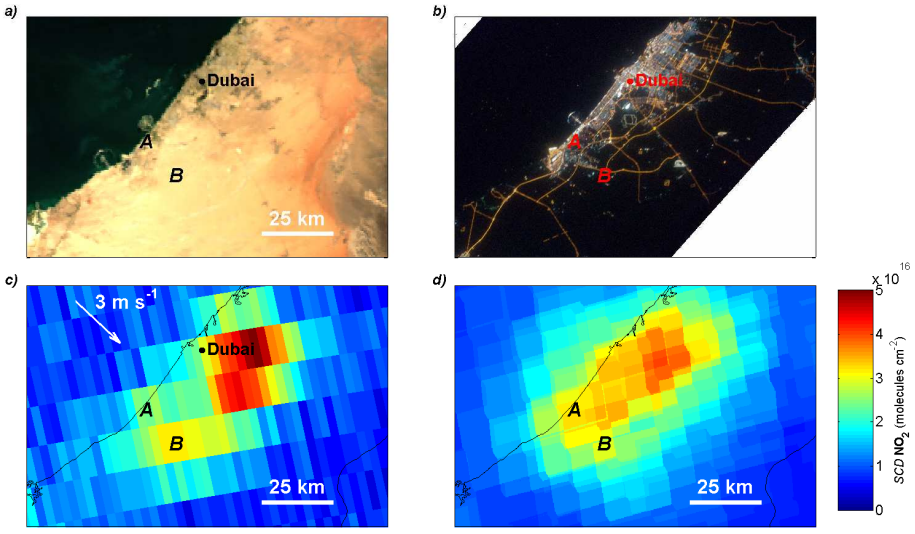

Fig. 4. **(a)** True color image from Aqua-MODIS on 21 November 2004. **(b)** Nighttime image (courtesy of the Image Science & Analysis Laboratory, NASA Johnson Space Center, ISS020-E-39932) captured aboard the International Space Station over Dubai, UAE, on 11 September 2009 at 02:00 a.m. LST. **(c)** Slant column NO_2 retrieved from a single overpass on November 21, 2004 for individual pixels and **(d)** a six-orbit, area-weighted average of slant column NO_2 retrieved from six operational-scale orbits (Table 1). Panels **(a)** and **(b)** highlight the locations of the Jebel Ali Free Zone and a point on the downwind transect. The white arrow in **(c)** indicates the direction and magnitude of winds observed at the Sharjah and Dubai International Airports at midday on 21 November 2004 (NOAA NCDC DS3505).

spatial resolution maps of atmospheric NO_2 over megacities and large power plants, or in accurately identifying the location of relatively small NO_x emission sources.

6 Case study over Dubai, UAE

In Fig. 4, we compare slant column NO_2 retrieved from a super-zoom overpass of Dubai with that retrieved from six operational-resolution overpasses (Table 1). We choose Dubai because the dataset is relatively simple to interpret. Dubai is an isolated source of NO_x advected over a highly reflective, relatively homogenous desert surface.

The observed NO_2 enhancement is approximately 75 km SW–NE by 40 km SE–NW (Fig. 4c), about two times the size of the Dubai metropolitan area (Fig. 4b). Within the observed plume, slant column NO_2 is highly variable, with differences as much as 2×10^{16} molecules cm^{-2} ($\sim$50 %) over 4 cross-track pixels (12 km) or one row (13 km). Adding confidence to the super-zoom observations, the 6-day operational resolution average (Fig. 4d) captures the same shape of the plume (75×40 km^2), but is not able to capture the strong gradients observed by the super-zoom mode, the result of a coarser footprint and meteorological variability in the six-day average.

Due to the alignment of the OMI super-zoom footprint, variability of emissions along the Dubai coastline should be detectable. For example, the super-zoom mode observes an enhancement of slant column NO_2 directly over and downwind from the Jebel Ali Free Trade Zone (JAFTZ), a port and power generation center (A, B, Fig. 4b–c). The enhancement directly over JAFTZ (A) is not as large as the enhancement downwind (B) because the source is near the leeward edge of the 13 km OMI pixel, which dilutes the signal with that of the clean marine background. In addition, the winds were stagnant between 10:00 a.m. and noon, during which NO_2 presumably accumulated over the source (A) and was transported downwind (B) when the winds shifted inland at midday (3 m s^{-1}, 11 km h^{-1}). The six-day area-weighted average (Fig. 4d) is not able to distinguish JAFTZ from the dense urban core to the northeast.

These examples demonstrate a few advantages of utilizing measurements at higher spatial resolution than the current OMI (13×24 km^2) or GOME-2 (40×80 km^2) products. Future opportunities to provide this substantial advance in scientific capability include the proposed TROPOMI (7×7 km^2) (Veefkind et al., 2011) and GEOCAPE instruments (currently targeted at 8×8 or 4×4 km^2) (NRC, 2007). Such observations will enable the tracking of individual source regions within cities and allow for better assessment of chemistry in urban outflow.

7 Conclusions

We show that slant column NO_2 retrieved from the super-zoom mode of OMI captures significant spatial variability at scales much finer than the 13×24 km^2 operational footprint. We show that the uncertainty of the super-zoom observations is a factor of $\sqrt{8}$ larger than that retrieved at

operational scale, which is expected for 8 times fewer measurements dominated by random error. We take advantage of enhanced resolution of the super-zoom observations to distinguish large point sources near the Rihand Reservoir and to distinguish the Jebel Ali Free Trade Zone, a Dubai port and power generation center, from the Dubai urban center 30 km to the northeast.

Acknowledgements. This work was supported by NASA under Grant #NNX08AE566, and by NASA Headquarters under the NASA Earth and Space Science Fellowship Program – Grant NESSF09, and CARB under Grant #06-328. We acknowledge the use of Level 1 data from Aura-OMI from http://disc.sci.gsfc.nasa.gov/Aura/data-holdings/OMI. We thank NOAA-NCDC for providing non-commercial access to hourly observations of wind and temperature over Dubai, UAE, at http://cdo.ncdc.noaa.gov/. We appreciate the image provided by the Image Science & Analysis Laboratory, NASA Johnson Space Center,http://eol.jsc.nasa.gov/.

Edited by: U. Friess

References

Boersma, K. F., Eskes, H. J., Veefkind, J. P., Brinksma, E. J., van der A, R. J., Sneep, M., van den Oord, G. H. J., Levelt, P. F., Stammes, P., Gleason, J. F., and Bucsela, E. J.: Near-real time retrieval of tropospheric NO_2 from OMI, Atmos. Chem. Phys., 7, 2103–2118, doi:10.5194/acp-7-2103-2007, 2007.

Bogumil, K., Orphal, J., Burrows, J. P., and Flaud, J. M.: Vibrational progressions in the visible and near-ultraviolet absorption spectrum of ozone, Chem. Phys. Lett., 349, 241–248, 2001.

Bucsela, E. J., Celarier, E. A., Wenig, M. O., Gleason, J. F., Veefkind, J. P., Boersma, K. F., and Brinksma, E. J.: Algorithm for NO_2 vertical column retrieval from the Ozone Monitoring Instrument, IEEE T. Geosci. Remote, 44, 1245–1258, doi:10.1109/tgrs.2005.863715, 2006.

Celarier, E. A., Brinksma, E. J., Gleason, J. F., Veefkind, J. P., Cede, A., Herman, J. R., Ionov, D., Goutail, F., Pommereau, J. P., Lambert, J. C., van Roozendael, M., Pinardi, G., Wittrock, F., Schonhardt, A., Richter, A., Ibrahim, O. W., Wagner, T., Bojkov, B., Mount, G., Spinei, E., Chen, C. M., Pongetti, T. J., Sander, S. P., Bucsela, E. J., Wenig, M. O., Swart, D. P. J., Volten, H., Kroon, M., and Levelt, P. F.: Validation of Ozone Monitoring Instrument nitrogen dioxide columns, J. Geophys. Res.-Atmos., 113, D15s15, doi:10.1029/2007jd008908, 2008.

Chance, K. and Kurucz, R. L.: An improved high-resolution solar reference spectrum for earth's atmosphere measurements in the ultraviolet, visible, and near infrared, J. Quant. Spectrosc. Ra., 111, 1289–1295, doi:10.1016/j.jqsrt.2010.01.036, 2010.

Chance, K. V. and Spurr, R. J. D.: Ring effect studies: Rayleigh scattering, including molecular parameters for rotational Raman scattering, and the Fraunhofer spectrum, Appl. Optics, 36, 5224–5230, 1997.

Dobber, M., Kleipool, Q., Dirksen, R., Levelt, P., Jaross, G., Taylor, S., Kelly, T., Flynn, L., Leppelmeier, G., and Rozemeijer, N.: Validation of Ozone Monitoring Instrument Level 1b data products, J. Geophys. Res.-Atmos., 113, D15s06, doi:10.1029/2007JD008665, 2008.

Dobber, M. R., Dirksen, R. J., Levelt, P. F., Van den Oord, G. H. J., Voors, R. H. M., Kleipool, Q., Jaross, G., Kowalewski, M., Hilsenrath, E., Leppelmeier, G. W., de Vries, J., Dierssen, W., and Rozemeijer, N. C.: Ozone Monitoring Instrument calibration, IEEE T. Geosci. Remote, 44, 1209–1238, doi:10.1109/tgrs.2006.869987, 2006.

Harder, J. W. and Brault, J. W.: Atmospheric measurements of water vapor in the 442-nm region, J. Geophys. Res.-Atmos., 102, 6245–6252, doi:10.1029/96jd01730, 1997.

Heue, K.-P., Wagner, T., Broccardo, S. P., Walter, D., Piketh, S. J., Ross, K. E., Beirle, S., and Platt, U.: Direct observation of two dimensional trace gas distributions with an airborne Imaging DOAS instrument, Atmos. Chem. Phys., 8, 6707–6717, doi:10.5194/acp-8-6707-2008, 2008.

Jaegle, L., Steinberger, L., Martin, R. V., and Chance, K.: Global partitioning of NO_x sources using satellite observations: Relative roles of fossil fuel combustion, biomass burning and soil emissions, Faraday Discuss., 130, 407–423, 2005.

Kim, S. W., Heckel, A., McKeen, S. A., Frost, G. J., Hsie, E. Y., Trainer, M. K., Richter, A., Burrows, J. P., Peckham, S. E., and Grell, G. A.: Satellite-observed US power plant NO_x emission reductions and their impact on air quality, Geophys. Res. Lett., 33(5), L22812, doi:10.1029/2006gl027749, 2006.

Konovalov, I. B., Beekmann, M., Richter, A., and Burrows, J. P.: Inverse modelling of the spatial distribution of NO_x emissions on a continental scale using satellite data, Atmos. Chem. Phys., 6, 1747–1770, doi:10.5194/acp-6-1747-2006, 2006.

Levelt, P. F., Hilsenrath, E., Leppelmeier, G. W., van den Oord, G. H. J., Bhartia, P. K., Tamminen, J., de Haan, J. F., and Veefkind, J. P.: Science objectives of the Ozone Monitoring Instrument, IEEE T. Geosci. Remote, 44, 1199–1208, doi:10.1109/tgrs.2006.872336, 2006a.

Levelt, P. F., Van den Oord, G. H. J., Dobber, M. R., Malkki, A., Visser, H., de Vries, J., Stammes, P., Lundell, J. O. V., and Saari, H.: The Ozone Monitoring Instrument, IEEE T. Geosci. Remote, 44, 1093–1101, doi:10.1109/tgrs.2006.872333, 2006b.

Loughner, C. P., Lary, D. J., Sparling, L. C., Cohen, R. C., DeCola, P., and Stockwell, W. R.: A method to determine the spatial resolution required to observe air quality from space, IEEE T. Geosci. Remote, 45, 1308–1314, doi:10.1109/tgrs.2007.893732, 2007.

Martin, R. V., Jacob, D. J., Chance, K., Kurosu, T. P., Palmer, P. I., and Evans, M. J.: Global inventory of nitrogen oxide emissions constrained by space-based observations of NO_2 columns, J. Geophys. Res.-Atmos., 108, 4537, doi:10.1029/2003JD003453, 2003.

NRC: Earth Science and Applications from Space: National imperatives for the next decade and beyond, edited by: National Research Council of the National Academies, The National Academic Press, Washington, DC, 2007.

Platt, U. and Stutz, J.: Differential optical absorption spectroscopy principles and applications, Physics of earth and space environments, Springer Verlag, Berlin, Germany, 597 pp., 2008.

Richter, A., Burrows, J. P., Nuss, H., Granier, C., and Niemeier, U.: Increase in tropospheric nitrogen dioxide over China observed from space, Nature, 437, 129–132, doi:10.1038/nature04092, 2005.

Russell, A. R., Valin, L. C., Bucsela, E. J., Wenig, M. O., and Cohen, R. C.: Space-based constraints on spatial and temporal patterns of NO_x emissions in California, 2005–2008, Environ. Sci.

Technol., 44, 3608–3615, doi:10.1021/es903451j, 2010.

Schoeberl, M. R., Douglass, A. R., Hilsenrath, E., Bhartia, P. K., Beer, R., Waters, J. W., Gunson, M. R., Froidevaux, L., Gille, J. C., Barnett, J. J., Levelt, P. E., and DeCola, P.: Overview of the EOS Aura mission, IEEE T. Geosci. Remote, 44, 1066–1074, doi:10.1109/tgrs.2005.861950, 2006.

Toenges-Schuller, N., Stein, O., Rohrer, F., Wahner, A., Richter, A., Burrows, J. P., Beirle, S., Wagner, T., Platt, U., and Elvidge, C. D.: Global distribution pattern of anthropogenic nitrogen oxide emissions: Correlation analysis of satellite measurements and model calculations, J. Geophys. Res.-Atmos., 111, D05312, doi:10.1029/2005JD006068, 2006.

Valin, L. C., Russell, A. R., Hudman, R. C., and Cohen, R. C.: Effects of model spatial resolution on the interpretation of satellite NO_2 observations, Atmos. Chem. Phys. Discuss., 11, 20245–20265, doi:10.5194/acpd-11-20245-2011, 2011.

Van den Oord, G. H. J., Rozemeijer, N. C., Schenkelaars, V., Levelt, P. F., Dobber, M. R., Voors, R. H. M., Claas, J., De Vries, J., Ter Linden, M., De Haan, C., and de Berg, T. V.: OMI level 0 to 1b processing and operational aspects, IEEE T. Geosci. Remote, 44, 1380–1397, doi:10.1109/tgrs.2006.872935, 2006.

Vandaele, A. C., Hermans, C., Fally, S., Carleer, M., Colin, R., Merienne, M. F., Jenouvrier, A., and Coquart, B.: High-resolution Fourier transform measurement of the NO_2 visible and near-infrared absorption cross sections: Temperature and pressure effects, J. Geophys. Res.-Atmos., 107, 434, doi:10.1029/2001jd000971, 2002.

Veefkind, J. P., Aben, I., McMullan, K., Förster, H., de Vries, J., Otter, G., Claas, J., Eskes, H., de Haan, J. P., Kleipool, Q., van Weele, M., Hasekamp, O. P., Hoogeveen, R., Landgraf, J., Snel, R., Tol, P., Ingmann, P., Voors, R., Kruizinga, B., Vink, R., Visser, H., and Levelt, P. F.: TROPOMI on the ESA Sentinel-5 Precursor: a GMES mission for Global Observations of the Atmospheric Composition for Climate, Air Quality and Ozone Layer Applications, Remote Sens. Environ., accepted, 2011.

Wenig, M., Jahne, B. J., and Platt, U.: Operator representation as a new differential optical absorption spectroscopy formalism, Appl. Optics, 44, 3246–3253, 2005.